Modeling of underwater swimming manipulators ⋆

J. Sverdrup-Thygeson * **E. Kelasidi** * **K. Y. Pettersen** * **J. T. Gravdahl** **

* *Centre for Autonomous Marine Operations and Systems, Department of Engineering Cybernetics, NTNU, Norwegian University of Science and Technology, Trondheim, Norway, (e-mail: {Jorgen.Sverdrup-Thygeson, Eleni.Kelasidi, Kristin.Y.Pettersen}@itk.ntnu.no)*
** *Department of Engineering Cybernetics, NTNU, Norwegian University of Science and Technology, Trondheim, Norway, (e-mail: Tommy.Gravdahl@itk.ntnu.no)*

Abstract: For several decades, the traditional ROV has been the workhorse used for any kind of subsea operations. The industry is now facing an important shift towards more economical and more efficient operations on subsea installations. To this end, there has been an increasing interest in smaller and lighter vehicles capable of performing autonomous tasks. In this paper we present the underwater swimming manipulator (USM), a hyper-redundant AUV with the potential to replace traditional ROVs and AUVs for routine inspection and lighter intervention tasks. We develop a mathematical model of the USM, including both kinematics and dynamic equations of motion. In addition, we present a generic force allocation method for USMs and the derivation of the configuration dependent force allocation matrix. The applicability of the proposed allocation method for path following control of USMs are demonstrated through computer simulations.

Keywords: Underwater Swimming Manipulator (USM), modeling of USM, force allocation for USM

1. INTRODUCTION

The oil and gas industry has been a key player in the development of a range of advanced technological solutions. In the last decade, there has been an increasing focus on subsea installations and operations, and along with that, new and extended requirements for subsea inspection, maintenance, and repair (IMR). These subsea operations have largely been performed using remotely operated vehicles (ROVs) equipped with one or more manipulator arms (Marani et al., 2009), also referred to as underwater vehicle manipulator systems (UVMS) (Fossen, 1991; Schjølberg and Fossen, 1994; Antonelli, 2014).

Traditional ROVs are large, heavy, expensive to operate, and require constant supervision. The time to mobilize and deploy them is also quite long. Consequently, the industry has recognized the need for less costly, small, lightweight, and autonomous units that can perform routine inspection tasks at subsea oil and gas installations and even carry out light intervention (Gilmour et al., 2012). In particular, there has been an increasing interest for developing autonomous underwater vehicles (AUVs) with hovering capabilities that can be used for inspection of subsea structures. Although the end goal is to also provide intervention capabilities, today they are used for inspection tasks only. The Subsea 7 autonomous inspection vehicle (AIV), Sabertooth by SAAB, and the HAUV produced by Bluefin Robotics are some examples. Benefits of this type of AUVs are easier transportation and deployment, precise maneuverability, and ability to operate in confined areas. Also, since they are untethered they are less likely to interfere with subsea operations. Some AUVs used for research have been equipped with small robotic arms to serve as intervention AUVs (I-AUVs). The dexterity of these manipulator equipped AUVs is however quite crude. A review of the state of the art for I-AUVs is given in Ridao et al. (2014).

The underwater swimming manipulator (USM) studied in this paper represents an alternative solution for various operations to be performed in an underwater environment since it has the potential to overcome the challenges mentioned for ROVs/AUVs. Essentially, a USM is a hyper-redundant underwater snake robot (USR) equipped with additional effectors, such as a stern propeller and tunnel thrusters along the body of the snake robot. A USR is a slender, articulated structure consisting of serially connected joint modules, with ability to swim like a biological eel. In other words, a USM is a crossover between a typical ROV/AUV and a USR. The USM has the ability to perform its own locomotion and at the same time serve as a manipulator. In particular, with its slender and articulated body, the USM is able to access even the most narrow parts of a subsea installation, areas which have previously been inaccessible due to the size of most ROVs/AUVs. The articulated body can be used as a typical robotic arm and the high number of links and joints yields a hyper-redundant design that outperforms traditional UVMS or manipulator equipped AUVs in terms of flexibility and dexterity.

Mathematical modelling, analysis and control of USMs present new challenges compared to ROVs and AUVs. Mathematical models for simulation of USR motion including hydrodynamic effects are derived in Kelasidi et al. (2014b), Kelasidi et al. (2014a), McIsaac and Ostrowski (1999), Khalil et al. (2007) and Porez et al. (2014). The methodology adopted in Kelasidi et al. (2014b) is similar to that used in Liljebäck et al. (2013) for land-based snake robots.

All these modelling approaches consider a snake robot having the identical properties for all the links of the robot (mass, length, etc.). In this paper we present extended models for the kinematics and dynamics of the USM by taking into account the different mass and different length of the links. In addition, we derive equations of motion combining the hydrodynamic model presented in Kelasidi et al. (2014b) with the forces produced by additional effectors such as propellers and thrusters. Note that the additional effectors can serve multiple purposes depending on the type and number of effectors added to the USM: a) the forward velocity of the USM can be increased, b) the agility and maneuverability can be improved by the ability to perform linear sideways displacements, c) the manipulation capability may be enhanced since the sinusoidal gait patterns normally used to generate propulsive forces for USRs may not be required, and d) the use of additional effectors can provide the USM with hovering capability which enables stationary inspection and intervention. We consider this as important contributions, since they have the potential to bridge the gap between USRs and other biologically inspired solutions on the one hand and conventional ROVs/AUVs on the other hand.

To the authors' best knowledge, this model is the first modeling approach that takes into account both the hydrodynamic effects and the forces produced from additional effectors. It is important to notice that the USR model presented in Kelasidi et al. (2014b) falls out as a special case, by considering a robot with the same link length and link mass for all links and setting the additional effector forces to zero. Hence, the model of the USM presented in this paper is an extension of the USR model in Kelasidi et al. (2014b), and comprises both USRs and USMs operating in an underwater environment. In addition to providing completeness, this also makes the model applicable for unified control methods for USRs and USMs.

In addition to presenting the mathematical model of the USM, we will in this paper discuss a generic force allocation problem for hyper-redundant structures such as USMs. This is a novel and complex problem, due to the high number of links, and since the articulated structure and joint motion affect the relative position between the added effectors and the center of mass (CM) of the USM. In particular, we develop a generic 2D force allocation matrix for USMs, which maps the individual additional effector forces to forces and moments on the CM of the USM.

Furthermore, we present an approach for path following control of USMs using the proposed force allocation method to distribute the required control efforts among the actuators. Simulation results are presented to support this. The proposed approach is applicable both with and without undulating motion, and can therefore be viewed as an extension of the path following control algorithm for USRs based on undulating motion presented in Kelasidi et al. (2014a,c). The primary advantage of the method proposed in this paper compared to Kelasidi et al. (2014a,c) is the possibility to increase the forward velocity and therefore obtain faster convergence to the desired path. Both methods use a line-of-sight algorithm for heading control. To our best knowledge, force allocation has not been used to solve the path following control problem for USMs in previous literature.

The paper is organized as follows. In Section 2 the mathematical model describing the kinematics and dynamics of the USM is derived. A generic force allocation method applicable to path following control of USMs and the corresponding force allocation matrix are presented in Section 3. Simulation results are presented in Section 4, while the conclusions and some options for future research are given in Section 5.

2. MODELLING OF A USM

In this section we derive the mathematical model describing the kinematics and dynamics of the USM. In particular, the kinematic equations are developed for 2D based on the method outlined in Liljebäck et al. (2013) for land-based snake robots and later modified in Kelasidi et al. (2014b) for underwater snake robots. We modify the kinematic equations and the equations of motion developed for a USR in Kelasidi et al. (2014b) to accommodate the different mass and length of each link, and combine them with the forces from additional effectors, such as stern propellers and tunnel thrusters.

2.1 Notation

We consider a USM consisting of n rigid links, connected by $n-1$ motorized joints, moving fully submerged in a 2D virtual horizontal plane. The USM is equipped with r additional effectors producing forces and moments on the CM of the USM. The length of each link is defined as $2l_i$, where $i = 1,...,n$ is the link number. As opposed to Kelasidi et al. (2014b) and Liljebäck et al. (2013), we take into consideration that the links may have different mass and length depending on the module configuration of the USM. We define the following diagonal matrices for mass, length, and inertia, respectively

$$\mathbf{M} = \text{diag}([m_1 \ \cdots \ m_n]) \in \mathbb{R}^{n \times n}, \mathbf{L} = \text{diag}([l_1 \ \cdots \ l_n]) \in \mathbb{R}^{n \times n},$$
$$\mathbf{J} = \text{diag}([j_1 \ \cdots \ j_n]) \in \mathbb{R}^{n \times n}.$$

The total mass of the USM is $m_t = \sum_{i=1}^{n} m_i$, and we make the following assumption about the mass distribution:

Assumption 1. The mass of each link is uniformly distributed.

Remark 1. Assumption 1 implies that the CM of each link is located at the midpoint of the link.

In this paper, we modify the notation used in Kelasidi et al. (2014b) and group the joint and the global link angles in the vectors $\mathbf{q} = [q_1,...,q_{n-1}]^T \in \mathbb{R}^{n-1}$ and $\psi = [\psi_1,...,\psi_n]^T \in \mathbb{R}^n$, respectively. The kinematics and the forces and torques acting on each link are illustrated in Fig. 1a and 1b, respectively. Symbols used in the subsequent sections are defined in Table I. We also define the following vectors and matrices for use in later sections:

$$\mathbf{A} = \begin{bmatrix} 1 & 1 & & \\ & \ddots & \ddots & \\ & & 1 & 1 \end{bmatrix} \in \mathbb{R}^{(n-1) \times n}, \mathbf{D} = \begin{bmatrix} 1 & -1 & & \\ & \ddots & \ddots & \\ & & 1 & -1 \end{bmatrix} \in \mathbb{R}^{(n-1) \times n},$$

$$\mathbf{e} = \begin{bmatrix} 1 & \cdots & 1 \end{bmatrix}^T \in \mathbb{R}^n, \mathbf{E} = \begin{bmatrix} \mathbf{e} & \mathbf{0}_{n \times 1} \\ \mathbf{0}_{n \times 1} & \mathbf{e} \end{bmatrix} \in \mathbb{R}^{2n \times 2},$$

$$\sin \psi = \begin{bmatrix} \sin \psi_1 & \cdots & \sin \psi_n \end{bmatrix}^T \in \mathbb{R}^n, \mathbf{S}_\psi = \text{diag}(\sin \psi) \in \mathbb{R}^{n \times n},$$

$$\cos \psi = \begin{bmatrix} \cos \psi_1 & \cdots & \cos \psi_n \end{bmatrix}^T \in \mathbb{R}^n, \mathbf{C}_\psi = \text{diag}(\cos \psi) \in \mathbb{R}^{n \times n},$$

$$\text{sgn} \psi = \begin{bmatrix} \text{sgn} \psi_1 & \cdots & \text{sgn} \psi_n \end{bmatrix}^T \in \mathbb{R}^n,$$

$$\dot{\psi}^2 = \begin{bmatrix} \dot{\psi}_1^2 & \cdots & \dot{\psi}_n^2 \end{bmatrix}^T \in \mathbb{R}^n.$$

2.2 Kinematics of the USM

The global frame position $\mathbf{p}_{\text{CM}} \in \mathbb{R}^2$ of the CM of the USM is defined as

$$\mathbf{p}_{\mathrm{CM}} = \begin{bmatrix} p_x \\ p_y \end{bmatrix} = \begin{bmatrix} \dfrac{1}{m_t} \sum_{i=1}^{n} m_i x_i \\ \dfrac{1}{m_t} \sum_{i=1}^{n} m_i y_i \end{bmatrix} = \dfrac{1}{m_t} \begin{bmatrix} \mathbf{e}^T \mathbf{M} \mathbf{X} \\ \mathbf{e}^T \mathbf{M} \mathbf{Y} \end{bmatrix}. \quad (1)$$

where (x_i, y_i), $i = 1, \dots, n$ are the coordinates of the CM of link i in the global frame. Note that this definition is valid due to Assumption 1. The rotation matrix between the frame of link i and the global frame is

$$\mathbf{R}_{\mathrm{link},i}^{\mathrm{global}} = \begin{bmatrix} \cos \psi_i & -\sin \psi_i \\ \sin \psi_i & \cos \psi_i \end{bmatrix}. \quad (2)$$

We adopt the Cartesian notation as used in Liljebäck et al. (2013) and express the holonomic constraints for the joints in matrix form as

$$\mathbf{DX} + \mathbf{AL} \cos \psi = \mathbf{0}, \quad \mathbf{DY} + \mathbf{AL} \sin \psi = \mathbf{0}, \quad (3a)$$

taking into account the different length of the links. We find the kinematic equations for the position of the individual links by combining (3) and (1):
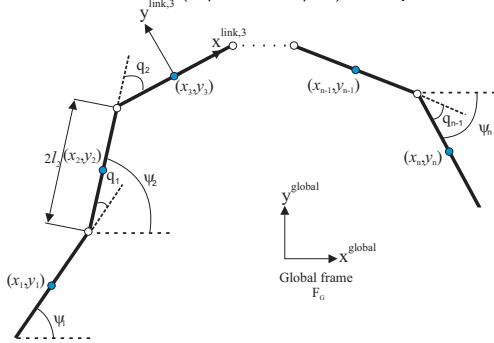
$$\mathbf{X} = -\mathbf{K}^T \cos \psi + \mathbf{e} p_x, \quad \mathbf{Y} = -\mathbf{K}^T \sin \psi + \mathbf{e} p_y, \quad (4a)$$

where $\mathbf{K} = \mathbf{LA}^T (\mathbf{DM}^{-1} \mathbf{D}^T)^{-1} \mathbf{DM}^{-1} \in \mathbb{R}^{n \times n}$. The linear velocities of the links are given by
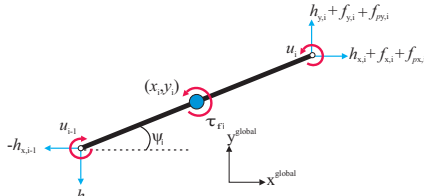
$$\dot{\mathbf{X}} = \mathbf{K}^T \mathbf{S}_\psi \dot{\psi} + \mathbf{e} \dot{p}_x, \quad \dot{\mathbf{Y}} = -\mathbf{K}^T \mathbf{C}_\psi \dot{\psi} + \mathbf{e} \dot{p}_y. \quad (5)$$

The linear accelerations of the links are found by differentiating the velocity of the individual links (5) with respect to time, which gives

$$\ddot{\mathbf{X}} = \mathbf{K}^T \left(\mathbf{C}_\psi \dot{\psi}^2 + \mathbf{S}_\psi \ddot{\psi} \right) + \mathbf{e} \ddot{p}_x,$$
$$\ddot{\mathbf{Y}} = \mathbf{K}^T \left(\mathbf{S}_\psi \dot{\psi}^2 - \mathbf{C}_\psi \ddot{\psi} \right) + \mathbf{e} \ddot{p}_y. \quad (6)$$

(a) Kinematic parameters

(b) Forces and torques acting on each link

Fig. 1. Underwater swimming manipulator

2.3 Hydrodynamic model of the USM

Regarding the hydrodynamic model, in Kelasidi et al. (2014b) it is shown that the fluid forces on all links can be expressed in vector form as

$$\mathbf{f} = \begin{bmatrix} \mathbf{f}_x \\ \mathbf{f}_y \end{bmatrix} = \begin{bmatrix} \mathbf{f}_{\mathbf{A_x}} \\ \mathbf{f}_{\mathbf{A_y}} \end{bmatrix} + \begin{bmatrix} \mathbf{f}_{\mathbf{D_x}}^{\mathrm{I}} \\ \mathbf{f}_{\mathbf{D_y}}^{\mathrm{I}} \end{bmatrix} + \begin{bmatrix} \mathbf{f}_{\mathbf{D_x}}^{\mathrm{II}} \\ \mathbf{f}_{\mathbf{D_y}}^{\mathrm{II}} \end{bmatrix}. \quad (7)$$

The vectors $\mathbf{f}_{\mathbf{A_x}}$ and $\mathbf{f}_{\mathbf{A_y}}$ represent the effects from added mass forces and are expressed as

Table I. Definition of mathematical symbols

Symbol	Description	Vector
n	The number of links	
l_i	The half length of a link	$\mathbf{L} \in \mathbb{R}^{n \times n}$
m_i	Mass of each link	$\mathbf{M} \in \mathbb{R}^{n \times n}$
j_i	Moment of inertia of each link	$\mathbf{J} \in \mathbb{R}^{n \times n}$
ψ_i	Angle between link i and the global x axis	$\psi \in \mathbb{R}^n$
q_i	Angle of joint i	$\mathbf{q} \in \mathbb{R}^{n-1}$
(x_i, y_i)	Global coordinates of the CM of link i	$\mathbf{X}, \mathbf{Y} \in \mathbb{R}^n$
(p_x, p_y)	Global coordinates of the CM of the robot	$\mathbf{p}_{\mathrm{CM}} \in \mathbb{R}^2$
u_i	Actuator torque of joint between link i and link $i+1$	$\mathbf{u} \in \mathbb{R}^{n-1}$
u_{i-1}	Actuator torque of joint between link i and link $i-1$	$\mathbf{u} \in \mathbb{R}^{n-1}$
$(f_{x,i}, f_{y,i})$	Fluid force on link i	$\mathbf{f}_x, \mathbf{f}_y \in \mathbb{R}^n$
$(f_{px,i}, f_{py,i})$	Added force on link i	$\mathbf{f}_{px}, \mathbf{f}_{py} \in \mathbb{R}^n$
τ_{fi}	Fluid torque on link i	$\tau_f \in \mathbb{R}^n$
$(h_{x,i}, h_{y,i})$	Joint constraint force on link i from link $i+1$	$\mathbf{h}_x, \mathbf{h}_y \in \mathbb{R}^{n-1}$
$-(h_{x,i-1}, h_{y,i-1})$	Joint constraint force on link i from link $i-1$	$\mathbf{h}_x, \mathbf{h}_y \in \mathbb{R}^{n-1}$

$$\begin{bmatrix} \mathbf{f}_{\mathbf{A_x}} \\ \mathbf{f}_{\mathbf{A_y}} \end{bmatrix} = - \begin{bmatrix} \mu \left(\mathbf{S}_\psi \right)^2 & -\mu \mathbf{S}_\psi \mathbf{C}_\psi \\ -\mu \mathbf{S}_\psi \mathbf{C}_\psi & \mu \left(\mathbf{C}_\psi \right)^2 \end{bmatrix} \begin{bmatrix} \ddot{\mathbf{X}} \\ \ddot{\mathbf{Y}} \end{bmatrix}$$
$$- \begin{bmatrix} -\mu \mathbf{S}_\psi \mathbf{C}_\psi & -\mu \left(\mathbf{S}_\psi \right)^2 \\ \mu \left(\mathbf{C}_\psi \right)^2 & \mu \mathbf{S}_\psi \mathbf{C}_\psi \end{bmatrix} \begin{bmatrix} \mathbf{V}_x^a \\ \mathbf{V}_y^a \end{bmatrix} \dot{\psi}, \quad (8)$$

where $\mu = \mathrm{diag}\,(\mu_1, \dots, \mu_n) \in \mathbb{R}^{n \times n}$, $\mathbf{V}_x^a = \mathrm{diag}\,(V_{x,1}, \dots, V_{x,n}) \in \mathbb{R}^{n \times n}$, $\mathbf{V}_y^a = \mathrm{diag}\,(V_{y,1}, \dots, V_{y,n}) \in \mathbb{R}^{n \times n}$ and $[V_{x,i}, V_{y,i}]^T$ is the ocean current velocity expressed in inertial frame coordinates. The drag forces on the USM are given by

$$\begin{bmatrix} \mathbf{f}_{\mathbf{D_x}}^{\mathrm{I}} \\ \mathbf{f}_{\mathbf{D_y}}^{\mathrm{I}} \end{bmatrix} = - \begin{bmatrix} \mathbf{c}_t \mathbf{C}_\psi & -\mathbf{c}_n \mathbf{S}_\psi \\ \mathbf{c}_t \mathbf{S}_\psi & \mathbf{c}_n \mathbf{C}_\psi \end{bmatrix} \begin{bmatrix} \mathbf{V}_{r_x}^{\mathrm{link}} \\ \mathbf{V}_{r_y}^{\mathrm{link}} \end{bmatrix}, \quad (9)$$

$$\begin{bmatrix} \mathbf{f}_{\mathbf{D_x}}^{\mathrm{II}} \\ \mathbf{f}_{\mathbf{D_y}}^{\mathrm{II}} \end{bmatrix} = - \begin{bmatrix} \mathbf{c}_t \mathbf{C}_\psi & -\mathbf{c}_n \mathbf{S}_\psi \\ \mathbf{c}_t \mathbf{S}_\psi & \mathbf{c}_n \mathbf{C}_\psi \end{bmatrix} \mathrm{sgn} \left(\begin{bmatrix} \mathbf{V}_{r_x}^{\mathrm{link}} \\ \mathbf{V}_{r_y}^{\mathrm{link}} \end{bmatrix} \right) \begin{bmatrix} (\mathbf{V}_{r_x}^{\mathrm{link}})^2 \\ (\mathbf{V}_{r_y}^{\mathrm{link}})^2 \end{bmatrix}, \quad (10)$$

where $\mathbf{c}_t = \mathrm{diag}\,(c_{t,1}, \dots, c_{t,n}) \in \mathbb{R}^{n \times n}$, $\mathbf{c}_n = \mathrm{diag}\,(c_{n,1}, \dots, c_{n,n}) \in \mathbb{R}^{n \times n}$, and $\mathbf{f}_{\mathbf{D_x}}^{\mathrm{I}}$, $\mathbf{f}_{\mathbf{D_y}}^{\mathrm{I}}$ and $\mathbf{f}_{\mathbf{D_x}}^{\mathrm{II}}$, $\mathbf{f}_{\mathbf{D_y}}^{\mathrm{II}}$ represent the effects from the linear and nonlinear drag forces, respectively. The velocities of the links relative to the ocean current velocity represented in the link frames are given by

$$\begin{bmatrix} \mathbf{V}_{r_x}^{\mathrm{link}} \\ \mathbf{V}_{r_y}^{\mathrm{link}} \end{bmatrix} = \begin{bmatrix} \mathbf{C}_\psi & \mathbf{S}_\psi \\ -\mathbf{S}_\psi & \mathbf{C}_\psi \end{bmatrix} \begin{bmatrix} \dot{\mathbf{X}} - \mathbf{V}_x \\ \dot{\mathbf{Y}} - \mathbf{V}_y \end{bmatrix}. \quad (11)$$

In addition, the fluid torques on all links are

$$\tau_f = -\mathbf{\Lambda}_1 \ddot{\psi} - \mathbf{\Lambda}_2 \dot{\psi} - \mathbf{\Lambda}_3 \dot{\psi} |\dot{\psi}|, \quad (12)$$

where $\mathbf{\Lambda}_1 = \mathrm{diag}\,(\lambda_{1,1}, \dots, \lambda_{1,n}) \in \mathbb{R}^{n \times n}$, $\mathbf{\Lambda}_2 = \mathrm{diag}\,(\lambda_{2,1}, \dots, \lambda_{2,n}) \in \mathbb{R}^{n \times n}$ and $\mathbf{\Lambda}_3 = \mathrm{diag}\,(\lambda_{3,1}, \dots, \lambda_{3,n}) \in \mathbb{R}^{n \times n}$. The coefficients $c_{t,i}$, $c_{n,i}$, $\lambda_{2,i}$, $\lambda_{3,i}$ represent the drag parameters due to the pressure difference between the two sides of the body, and the parameters μ_i, $\lambda_{1,i}$ represent the added mass of the fluid carried by the moving body.

Remark 2. In this paper the hydrodynamic parameters are adapted in order to consider the different length of the links.

2.4 Added effectors

The forces and moments on the CM of the USM created by the added effectors are dependent on the line of action of these forces. We make the following assumption about the line of action of the additional effector forces:

Assumption 2. The forces from the added effectors have line of action through the center of mass of each actuated link.

Remark 3. Assumption 2 implies that the added forces will not directly affect the individual torque balances of the links. However, the added forces will affect the orientation of each link indirectly through the joint constraint forces $\mathbf{h}_x \in \mathbb{R}^{n-1}$ and $\mathbf{h}_y \in \mathbb{R}^{n-1}$ derived later in this section.

Using the rotation matrix in (2) we find the added effector forces of link i, expressed in the global frame:

$$\mathbf{f}_{p,i} = \begin{bmatrix} f_{px,i} \\ f_{py,i} \end{bmatrix} = \mathbf{R}_{\text{link},i}^{\text{global}} \mathbf{R}_{\alpha,i} \begin{bmatrix} f_{p,i} \\ 0 \end{bmatrix} = \begin{bmatrix} \cos(\psi_i + \alpha_i) \\ \sin(\psi_i + \alpha_i) \end{bmatrix} f_{p,i} \quad (13)$$

where $\mathbf{R}_{\alpha,i} = \begin{bmatrix} \cos\alpha_i & -\sin\alpha_i \\ \sin\alpha_i & \cos\alpha_i \end{bmatrix}$ represents the orientation of the added force vector with respect to the local reference frame of link i, and $f_{p,i}$ are the scalar magnitudes of the added forces of the same link. The scalar forces are grouped in the vector $\mathbf{f}_p = \left[f_{p,k_1}, \ldots, f_{p,k_r} \right]^T \in \mathbb{R}^r$, where r is the total number of additional effectors and $k_i \in \{1, \ldots, n\}$. We define the configuration vectors $\mathbf{b}_x$ and $\mathbf{b}_y$ using the x and y components from (13)

$$\mathbf{b}_x = [\cos(\psi_{k_1} + \alpha_{k_1}) \ \cos(\psi_{k_2} + \alpha_{k_2}) \ \ldots \ \cos(\psi_{k_r} + \alpha_{k_r})]^T \tag{14a}$$

$$\mathbf{b}_y = [\sin(\psi_{k_1} + \alpha_{k_1}) \ \sin(\psi_{k_2} + \alpha_{k_2}) \ \ldots \ \sin(\psi_{k_r} + \alpha_{k_r})]^T. \tag{14b}$$

The global frame added forces in (13) are then grouped in x and y vectors, respectively,

$$\mathbf{f}_{px} = \mathbf{B}_X^T \mathbf{f}_p \in \mathbb{R}^n, \qquad \mathbf{B}_X(\mathbf{b}_x) \in \mathbb{R}^{r \times n}, \tag{15a}$$

$$\mathbf{f}_{py} = \mathbf{B}_Y^T \mathbf{f}_p \in \mathbb{R}^n, \qquad \mathbf{B}_Y(\mathbf{b}_y) \in \mathbb{R}^{r \times n}. \tag{15b}$$

The number of rows of $\mathbf{b}_x$, $\mathbf{b}_y$, $\mathbf{B}_X$ and $\mathbf{B}_Y$ depend on the number of additional effectors.

Remark 4. The extended model with added effectors derived in this paper is general in the sense that it can be used for including any kind of added forces depending on the application. By including forces from fins or a caudal tail, it is possible to study the locomotion properties of USRs and robotic fish. If combined with forces from tunnel thrusters and a stern propeller, we can study the motion of a USM carrying out different applications in a subsea environment.

2.5 Equations of motion

The matrix representation of the force balance for all links with different link mass is expressed by

$$\mathbf{M}\ddot{\mathbf{X}} = \mathbf{D}^T \mathbf{h}_x + \mathbf{f}_x + \mathbf{f}_{px}, \quad \mathbf{M}\ddot{\mathbf{Y}} = \mathbf{D}^T \mathbf{h}_y + \mathbf{f}_y + \mathbf{f}_{py}, \tag{16a}$$

where $\mathbf{f}_{px}$ and $\mathbf{f}_{py}$ are the forces from the additional effectors expressed in (15). By differentiating (1) and inserting (16), the joint constraint forces cancel out, and the translational motion of the CM of the USM can be written as

$$m_t \ddot{p}_x = \mathbf{e}^T (\mathbf{f}_x + \mathbf{f}_{px}), \quad m_t \ddot{p}_y = \mathbf{e}^T (\mathbf{f}_y + \mathbf{f}_{py}), \tag{17a}$$

where m_t is the total mass of the USM. Inserting (7) and (8) in (17) yields the final equations for the acceleration of the CM

$$\begin{bmatrix} \ddot{p}_x \\ \ddot{p}_y \end{bmatrix} = -\mathbf{M}_p \begin{bmatrix} \mathbf{e}^T \mu \mathbf{S}_\psi^2 & -\mathbf{e}^T \mu \mathbf{S}_\psi \mathbf{C}_\psi \\ -\mathbf{e}^T \mu \mathbf{S}_\psi \mathbf{C}_\psi & \mathbf{e}^T \mu \mathbf{C}_\psi^2 \end{bmatrix} \begin{bmatrix} \mathbf{K}^T (\mathbf{C}_\psi \dot{\psi}^2 + \mathbf{S}_\psi \ddot{\psi}) \\ \mathbf{K}^T (\mathbf{S}_\psi \dot{\psi}^2 - \mathbf{C}_\psi \ddot{\psi}) \end{bmatrix}$$

$$- \mathbf{M}_p \begin{bmatrix} -\mathbf{e}^T \mu \mathbf{S}_\psi \mathbf{C}_\psi & -\mathbf{e}^T \mu \mathbf{S}_\psi^2 \\ \mathbf{e}^T \mu \mathbf{C}_\psi^2 & \mathbf{e}^T \mu \mathbf{S}_\psi \mathbf{C}_\psi \end{bmatrix} \begin{bmatrix} \mathbf{V}_x^a \\ \mathbf{V}_y^a \end{bmatrix} \dot{\psi}$$

$$+ \mathbf{M}_p \begin{bmatrix} \mathbf{e}^T (\mathbf{f}_{Dx} + \mathbf{f}_{px}) \\ \mathbf{e}^T (\mathbf{f}_{Dy} + \mathbf{f}_{py}) \end{bmatrix} \tag{18}$$

where

$$\mathbf{M}_p = \begin{bmatrix} m_{11} & m_{12} \\ m_{21} & m_{22} \end{bmatrix} = \begin{bmatrix} m_t + \mathbf{e}^T \mu \mathbf{S}_\psi^2 \mathbf{e} & -\mathbf{e}^T \mu \mathbf{S}_\psi \mathbf{C}_\psi \mathbf{e} \\ -\mathbf{e}^T \mu \mathbf{S}_\psi \mathbf{C}_\psi \mathbf{e} & m_t + \mathbf{e}^T \mu \mathbf{C}_\psi^2 \mathbf{e} \end{bmatrix}^{-1}$$

The joint constraint forces $\mathbf{h}_x$ and $\mathbf{h}_y$ are found by premultiplying (16) with $(\mathbf{DM}^{-1}\mathbf{D}^T)^{-1}\mathbf{DM}^{-1}$

$$\mathbf{h}_x = (\mathbf{DM}^{-1}\mathbf{D}^T)^{-1}(\mathbf{D}\ddot{\mathbf{X}} - \mathbf{DM}^{-1}(\mathbf{f}_x + \mathbf{f}_{px})) \tag{19a}$$

$$\mathbf{h}_y = (\mathbf{DM}^{-1}\mathbf{D}^T)^{-1}(\mathbf{D}\ddot{\mathbf{Y}} - \mathbf{DM}^{-1}(\mathbf{f}_y + \mathbf{f}_{py})). \tag{19b}$$

The torque balance for link i with different link length is expressed as

$$J\ddot{\psi}_i = u_i - u_{i-1} - l_i \sin\psi_i (h_{x,i} + h_{x,i-1}) + l_i \cos\psi_i (h_{y,i} + h_{y,i-1}) + \tau_{fi}. \tag{20}$$

Assembling the torque balance equations in matrix form and inserting (19) and the second derivative of (3) yields

$$\mathbf{J}\ddot{\psi} = \mathbf{D}^T \mathbf{u} - \mathbf{S}_\psi \mathbf{LA}^T \mathbf{h}_x + \mathbf{C}_\psi \mathbf{LA}^T \mathbf{h}_y + \tau_f$$
$$= \mathbf{D}^T \mathbf{u} - \mathbf{S}_\psi \mathbf{V}(\mathbf{C}_\psi \dot{\psi}^2 + \mathbf{S}_\psi \ddot{\psi}) + \mathbf{S}_\psi \mathbf{K}(\mathbf{f}_x + \mathbf{f}_{px}) \qquad (21)$$
$$+ \mathbf{C}_\psi \mathbf{V}(\mathbf{S}_\psi \dot{\psi}^2 - \mathbf{C}_\psi \ddot{\psi}) - \mathbf{C}_\psi \mathbf{K}(\mathbf{f}_y + \mathbf{f}_{py}) + \tau_f,$$

where $\mathbf{V} = \mathbf{LA}^T (\mathbf{DM}^{-1}\mathbf{D}^T)^{-1}\mathbf{AL}$ and τ_f is given from (12). Finally, we insert the equation for the added mass forces given by (8) and the linear accelerations of the links given by (6), and express the equations of motion as

$$\mathbf{M}_\psi \ddot{\psi} + \mathbf{W}_\psi \dot{\psi}^2 + \mathbf{V}_\psi \dot{\psi} + \Lambda_3 |\dot{\psi}|\dot{\psi} - \mathbf{K}_1 \mu (\mathbf{S}_\psi \mathbf{e}\ddot{p}_x - \mathbf{C}_\psi \mathbf{e}\ddot{p}_y)$$
$$+ \mathbf{S}_\psi \mathbf{K}(\mathbf{f}_{Dx} + \mathbf{f}_{px}) - \mathbf{C}_\psi \mathbf{K}(\mathbf{f}_{Dy} + \mathbf{f}_{py}) = \mathbf{D}^T \mathbf{u}, \tag{22}$$

where

$$\mathbf{M}_\psi = \mathbf{J} + \mathbf{V}_1 + \mathbf{K}_1 \mu \mathbf{K}_1^T + \Lambda_1, \quad \mathbf{W}_\psi = \mathbf{V}_2 - \mathbf{K}_1 \mu \mathbf{K}_2^T$$
$$\mathbf{V}_\psi = \Lambda_2 - \mathbf{K}_1 \mu (\mathbf{C}_\psi \mathbf{V}_x^a + \mathbf{S}_\psi \mathbf{V}_y^a)$$
$$\mathbf{K}_1 = \mathbf{S}_\psi \mathbf{KS}_\psi + \mathbf{C}_\psi \mathbf{KC}_\psi, \ \mathbf{K}_2 = \mathbf{S}_\psi \mathbf{KC}_\psi - \mathbf{C}_\psi \mathbf{KS}_\psi,$$
$$\mathbf{V}_1 = \mathbf{S}_\psi \mathbf{VS}_\psi + \mathbf{C}_\psi \mathbf{VC}_\psi, \ \mathbf{V}_2 = \mathbf{S}_\psi \mathbf{VC}_\psi - \mathbf{C}_\psi \mathbf{VS}_\psi.$$

Note that, as opposed to Kelasidi et al. (2014b), we obtain equations of motion that allow the links to have different length and mass. With a slight abuse of notation, we choose not to substitute (18) in (22) to maintain a compact notation and to recognize the structure of the equations.

Remark 5. It is interesting to note that the dynamic model for the USM in (18) and (22) presented in this paper takes into account linear and nonlinear drag forces, added mass, current effects, and also the forces produced from additional effectors. The USR model presented in Kelasidi et al. (2014b) falls out as a special case, by considering a robot with same link length and link mass for all links and setting the additional effector forces to zero. Hence, the model of the USM presented in this paper is an extension of the USR model in Kelasidi et al. (2014b), and comprise both USRs and USMs operating in an underwater environment.

3. FORCE ALLOCATION

In this section we present the generic force allocation concept for USMs. In addition, we derive the force allocation matrix for 2D applications, and discuss a specific force allocation method applicable for path following control of USMs.

A system is overactuated if it possesses more independent control inputs than degrees of freedom to be controlled. As such, a USM with additional effectors may be overactuated with respect to the task of controlling the position and orientation of the CM of the USM. In this paper, we restrict the force allocation problem to consider only the forces and torques produced by the additional effectors. We do not consider the joint motor torques applied for actuation of each individual joint in the force allocation algorithm. However, in order to utilize the advantage of the USM being a highly articulated structure, we investigate the possibility to use the motorized joints for heading control in combination with the force allocation method.

For an overactuated USM there are many different ways to distribute the control efforts among the effectors and yet obtain the same net forces and moments on the center of mass. Proper

force allocation is therefore required to do so in an optimal manner. Control allocation has been studied extensively in the context of motion control for surface vessels (Berge and Fossen, 1997; Johansen et al., 2008; Lindfors, 1993; Sørdalen, 1997; Webster and Sousa, 1999), and underwater vehicles (Fossen et al., 2008; Indiveri and Parlangeli, 2006), as well as in space-craft attitude control (Jin et al., 2006; Fu et al., 2011), and flight control systems (Oppenheimer et al., 2010; Durham, 1993). A recent survey on control allocation methods and applications is given in Johansen and Fossen (2013). Control allocation for articulated structures is much less studied. Coordination of actuators for articulated ground vehicles is investigated in terms of traction control in Uhlen et al. (2014), Andersson (2013) and yaw stability in Yang (2012), however, limited to 2 or 3 links.

A typical control allocation algorithm relies on input from a high-level motion control law producing a vector of virtual inputs, which in many cases is interpreted as the desired generalized forces and moments. The primary objective of the control allocation algorithm is then to distribute commands among the actuators such that the total forces and moments produced equals the desired virtual input (Johansen and Fossen, 2013).

Let m be the number of degrees of freedom to be controlled and r be the number of additional effectors. We define the force allocation matrix $\mathbf{T}(\psi) \in \mathbb{R}^{m \times r}$ with one column vector for each additional effector such that

$$\tau_{CM} = \mathbf{T}(\psi)\mathbf{f}_p, \tag{23}$$

where $\mathbf{f}_p = \left[f_{p,k_1}, \ldots, f_{p,k_r}\right]^T$ is the vector of scalar effector forces introduced in Section 2.4, and τ_{CM} is the total forces and moments exerted on the CM of the USM. When $r > m$ the matrix $\mathbf{T}(\psi)$ is non-square and the set of equations defined through (23) is underdetermined, which means that there is an infinite number of solutions $\mathbf{f}_p$ satisfying (23) given a vector τ_{CM} of desired forces and moments. This is a significant advantage, since it allows the force allocation problem to be formulated as an optimization problem that seeks to achieve secondary control objectives in addition to obtaining the commanded generalized forces.

Force allocation for articulated structures is a complex dynamic problem, not only due to the dynamic response of the effectors, but also because the point of attack and line of action of the effector forces change when the geometry of the USM is changed. The latter means that the relative position between the CM of the USM and the CM of each link is changed, which changes the allocation matrix. The allocation matrix will thus be a function of the link angles. This has similarities with control allocation for surface vessels with azimuth thrusters, where the allocation matrix depends on the azimuth thruster angles.

Since we here focus on the generic force allocation concept, we do not consider the dynamic models of the effectors.

Assumption 3. We assume that there is a static mapping from the control input to the forces produced by the effectors.

Remark 6. For certain types of effectors, assuming such a static mapping is acceptable, while other types of effectors have highly nonlinear dynamic characteristics. Due to the scope of this paper, including nonlinear dynamic effector characteristics is left for future work.

Furthermore, we assume that

Assumption 4. The servo motors controlling the joint angles are strong enough to maintain the body shape of the USM under the influence of the added effector forces.

Remark 7. Assumption 4 implies that the USM can be treated as a rigid body for any given body shape. As long as the servo motors for the joints are not actively used to alter the body shape, the USM will behave as a rigid body under the influence of the added effector forces.

3.1 The force allocation matrix

In this section we derive the force allocation matrix for 2D applications. The solution to the force allocation problem is an optimal distribution of effector forces with respect to a set of optimization criteria and possible constraints. This distribution is given by $\mathbf{T}(\psi)$ in (23), i.e. the mapping between the effector forces and the forces and moments acting on the CM of the USM. Since by Assumption 2 we assume that the additional effector forces are acting through the center of mass of each link, we write the total forces and moments exerted on the CM of the USM as

$$\tau_{CM} = \begin{bmatrix} F_{CM,x} \\ F_{CM,y} \\ M_{CM,z} \end{bmatrix} = \begin{bmatrix} \sum \mathbf{f}_{p,k_i} \\ \sum \mathbf{r}_{k_i} \times \mathbf{f}_{p,k_i} \end{bmatrix} = \begin{bmatrix} \mathbf{I}^{2x2} & \cdots & \mathbf{I}^{2x2} \\ [\mathbf{r}_{k_1}]_\times & \cdots & [\mathbf{r}_{k_r}]_\times \end{bmatrix} \begin{bmatrix} \mathbf{f}_{p,k_1} \\ \vdots \\ \mathbf{f}_{p,k_r} \end{bmatrix} \tag{24}$$

where $k_i \in \{1, ..., n\}$, $\mathbf{r}_{k_i} \in \mathbb{R}^2$ are the moment arm vectors from the CM of the USM to the CM of link k_i expressed in the global frame, $[\mathbf{r}_{k_i}]_\times$ is the skew symmetric form of $\mathbf{r}_{k_i}$, and $\mathbf{f}_{p,k_i}$ are the global frame effector forces acting on link k_i, given by (13).

The moment arm vectors are given by (4)

$$\mathbf{r}_i = -\begin{bmatrix} \mathbf{K}_i^T \cos \psi \\ \mathbf{K}_i^T \sin \psi \end{bmatrix}, \tag{25}$$

where $\mathbf{K}_i$ is the i'th column of the matrix $\mathbf{K}$. We insert (13) and (25) in (24) and reorganize the sequence of the force vector elements such that the x and y components are grouped together. This gives

$$\tau_{CM} = \begin{bmatrix} 1 & \cdots & 1 & 0 & \cdots & 0 \\ 0 & \cdots & 0 & 1 & \cdots & 1 \\ \mathbf{K}_1^T s\psi & \cdots & \mathbf{K}_n^T s\psi & -\mathbf{K}_1^T c\psi & \cdots & -\mathbf{K}_n^T c\psi \end{bmatrix} \begin{bmatrix} \mathbf{f}_{px} \\ \mathbf{f}_{py} \end{bmatrix}$$

$$= \begin{bmatrix} \mathbf{e}^T & \mathbf{0}^{1xn} \\ \mathbf{0}^{1xn} & \mathbf{e}^T \\ \mathbf{e}^T \mathbf{S}_\psi \mathbf{K} & -\mathbf{e}^T \mathbf{C}_\psi \mathbf{K} \end{bmatrix} \begin{bmatrix} \mathbf{B}_X^T \\ \mathbf{B}_Y^T \end{bmatrix} \mathbf{f}_p. \tag{26}$$

Consequently, the allocation matrix $\mathbf{T}(\psi)$ can be expressed as

$$\mathbf{T}(\psi) = \begin{bmatrix} \mathbf{b}_x^T \\ \mathbf{b}_y^T \\ \mathbf{e}^T \mathbf{S}_\psi \mathbf{K} \mathbf{B}_X^T - \mathbf{e}^T \mathbf{C}_\psi \mathbf{K} \mathbf{B}_Y^T \end{bmatrix}. \tag{27}$$

Remark 8. We see that the expression for the force allocation matrix in (27) is consistent with the corresponding forces and moments in equations (17) and (22).

3.2 Force allocation for path following of USMs

In this section, we present a method for path following control of USMs using the added effectors and not the common path following approach for USRs based on undulating motion. The path following control method proposed in this paper is a guidance-based control method. In particular, in order to follow the desired path, a desired heading angle is generated by the control algorithm and it is combined with a heading controller which is responsible for steering the USM towards and subsequently along the desired path. Note that for path following of USRs, a gait pattern controller is commonly used in order

to produce a sinusoidal motion pattern which propels the USR forward (Kelasidi et al., 2014a,c). This sinusoidal motion is not considered in the path following control method proposed in this paper. The added effectors produce the required forces to propel the USM forward, while the direction of the USM is controlled by combining the force allocation algorithm and the joint angles.

As it has already been mentioned, the force allocation subsystem relies on input from a high-level control law producing the desired forces and moments on the CM of the USM, $\tau_{CM,d}$. Thus, the force allocation method is not designed to compensate for defects or limitations in the control law. We assume that there exists a guidance system which determines a suitable path to follow. A standard PD controller, with controller gains k_p^{CM} and k_d^{CM}, is used to calculate the desired forces and moments, $\tau_{CM,d}$, to track the position and heading along the path

$$\tau_{CM,d} = k_d^{CM} \begin{bmatrix} \dot{p}_{x,ref} - \dot{p}_x \\ \dot{p}_{y,ref} - \dot{p}_y \\ 0 \end{bmatrix} + k_p^{CM} \begin{bmatrix} p_{x,ref} - p_x \\ p_{y,ref} - p_y \\ \bar{\psi}_{ref} - \bar{\psi} \end{bmatrix}. \qquad (28)$$

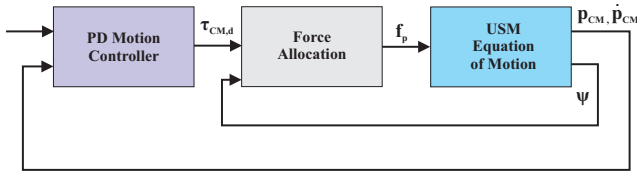Fig. 2 shows the different subsystems.

Fig. 2. System overview

Motivated by Kelasidi et al. (2014a); Liljebäck et al. (2013) we define the reference heading, $\bar{\psi}_{ref}$, using the line-of-sight (LOS) guidance law

$$\bar{\psi}_{ref} = -\arctan\left(\frac{p_y}{\Delta}\right), \qquad \Delta > 0, \qquad (29)$$

where Δ is the look-ahead-distance and p_y is the cross-track error from the path. We define the heading of the USM to be the head link angle

$$\bar{\psi} = \psi_n, \qquad (30)$$

instead of the average of the link angles as in Kelasidi et al. (2014b). The proposed LOS guidance law is commonly used for path following control of marine surface vessels and it has been used for path following of USRs in Kelasidi et al. (2014a). See more details in Kelasidi et al. (2014a). In this paper, we do not consider ocean current effects when solving the path following control problem. An integral line-of-sight guidance control law could be used in order to compensate for the effects of the ocean current, as in Kelasidi et al. (2014c).

The primary objective for the force allocation method proposed in this section is to distribute the efforts among the additional effectors to obtain the forces and moments required to maintain the desired heading and follow the path with nonzero forward velocity. When the USM is overactuated with respect to this task, then we can add secondary objectives to the force allocation problem. For path following with a USM, we conjecture that minimizing the effort of the additional effectors, i.e. minimizing the power consumption, is the most important. With minimum effort as the optimization criteria, we can formulate the unconstrained least-squares optimization problem as follows

$$\mathbf{J}_{cf} = \min_{\mathbf{f}_p} \left\{ \mathbf{f}_p^T \mathbf{W} \mathbf{f}_p \right\} \text{ subject to: } \tau_{CM,d} - \mathbf{T}(\psi)\mathbf{f}_p = 0 \qquad (31)$$

The explicit solution to this optimization problem is (Fossen and Sagatun, 1991)

$$\mathbf{f}_p = \mathbf{T}_W^\dagger \tau_{CM,d} \qquad (32)$$

where $\mathbf{T}_W^\dagger = \mathbf{W}^{-1}\mathbf{T}(\psi)^T (\mathbf{T}(\psi)\mathbf{W}^{-1}\mathbf{T}(\psi)^T)^{-1}$ is the generalized inverse and $\mathbf{W}$ is a matrix specifying the relative weighting between the additional effectors.

This method solves the unconstrained allocation problem. It does not take into account force saturation and possible rank deficiency of $\mathbf{T}(\psi)$. If $\mathbf{T}(\psi)$ looses rank, then $\mathbf{T}(\psi)\mathbf{W}^{-1}\mathbf{T}(\psi)^T$ becomes singular and non-invertible.

Remark 9. Note that since the force allocation matrix is derived as a function of the links angles ψ, the force allocation method is also applicable when the joint angles are controlled by an undulating motion pattern.

To obtain a smooth motion, we propose to combine the use of the additional effectors and the joint motors to control the heading of the USM, by setting all the joint angle references to

$$q_i^* = k_\psi(\bar{\psi} - \bar{\psi}_{ref}). \qquad (33)$$

The additional effectors contribute to the heading control through the desired moment $M_{CM,z}$ in (24) computed by the PD controller mentioned above. In addition, in order to make the joint angle q_i follow its reference signal q_i^*, a simple PD controller is used to determine the actuator torque control input of joint i:

$$u_i = k_p(q_i^* - q_i) - k_d\dot{q}_i, \quad i = 1,\dots,n-1, \qquad (34)$$

where $k_p > 0$ and $k_d > 0$ are the gains of the controller. The derivative part is included to damp high joint velocities.

In Section 4, closed-loop simulation results are presented using the method above.

4. SIMULATION RESULTS

In this section we apply the force allocation method for path following control proposed in Section 3 and show that the additional effector forces are effectively distributed and that the USM is able to follow the given path with the desired heading. The dynamic model presented in Section 2 were implemented in *Matlab*. The time evolution was calculated using the *ode23tb* solver with a relative and absolute error tolerance of 10^{-4}.

A USM was considered with $n = 16$ links, each one having length $2l_i = 0.14$ m and mass $m_i = 0.6597$ kg. The hydrodynamic related parameters $\mathbf{c}_t$, $\mathbf{c}_n$, μ, Λ_1, Λ_2, and Λ_3 were computed for the elliptic link section with major and minor diameters $2a = 2 \cdot 0.03$ m and $2b = 2 \cdot 0.05$ m, respectively. The fluid properties were assumed to be $\rho = 1000$ kg/m³ and $C_f = 0.03$, $C_D = 2$, $C_A = 1$, $C_M = 1$ and used to compute the parameters by using equations derived in Kelasidi et al. (2014b). The initial position of the CM was selected as $\mathbf{p}_{CM}(0) = [0,3]$ m, the parameter $k_\psi = 0.8$ and the parameter $\Delta = 2l_i n$ m. The PD controller parameters were chosen as $k_p^{CM} = 0.6$, $k_d^{CM} = 0.06$, $k_p = 20$, and $k_d = 10$.

In this paper, the main objective is to control the position of the center of mass in 2D, and the heading of the USM, a total of three degrees of freedom. Thus, the USM should be equipped with a minimum of three additional effectors, located such that the force allocation matrix maintains full row rank. In order to demonstrate the applicability of the proposed force allocation method, we perform simulations with three and five additional effectors, both with and without using the joint angles for heading control. The four different cases we have simulated in this paper are selected to validate the concept of LOS path following for a USM with additional effectors and

to highlight some important differences between the cases. The solution in (32) is optimal with respect to the total effort for the given effector configurations. In this paper, we do not aim at finding the optimal number and configuration of effectors, as this will likely depend on the environmental disturbances and the complexity of the path to follow. Also, we choose to simulate the special case of same length and same mass for all the links, since the main purpose of the simulation section is to demonstrate the LOS path following and the force allocation.

The simulations are carried out with two different effector configurations:

- **Configuration 1**: One tail effector at link 1 exerting force along the link x axis. Two additional effectors located at link number 3 and 14 exerting forces normal to the links.
- **Configuration 2**: One tail effector at link 1 exerting force along the link x axis. Four additional effectors located at link number 3, 6, 11, and 14 exerting forces normal to the links.

The four simulation cases are:

- **Case 1**: Effector configuration 1. Straight line path following with joint angle heading control.
- **Case 2**: Effector configuration 1. Straight line path following without joint angle heading control.
- **Case 3**: Effector configuration 2. Straight line path following with joint angle heading control.
- **Case 4**: Effector configuration 2. Straight line path following without joint angle heading control.

In all the cases, we see from Fig. 3 that the heading reference is followed, the cross-track error converges to zero, and the USM reaches and follows the given straight line path. Comparing cases 1 and 3 with cases 2 and 4, we notice that both the heading and the CM position converge faster when including the joint angles in the heading control. In cases 2 and 4 the USM behaves like a long and slender rigid body, not utilizing the inherent advantage of the articulated joints. Watching the visualization of the simulations in real-time also shows that using the joint angles for heading control produce a much smoother approach to the path. We expect that this will reduce the total drag forces, especially when performing turning motions. This expectation is supported by Fig. 4 which shows that the total effector effort is slightly higher for cases 2 and 4 when performing the initial turning motion towards the path.

Cases 3 and 4 show that including more effectors reduces the maximum effector effort. Since the force allocation method minimizes the total effort in a least-squares sense and selects the optimal distribution of forces, we conclude that for this case study it is advantageous to have more effectors. It should be noted, however, that the physical locations of the effectors along the body of the USM are significant for the distribution of the effector commands and the combined effort. We expect that the advantage of having more effectors becomes more pronounced when increasing the complexity of the path. Other benefits include redundancy with respect to fault tolerance and less chance of the matrix $\mathbf{T}(\psi)\mathbf{W}^{-1}\mathbf{T}(\psi)^T$ becoming singular. In the end, Fig. 3 and Fig. 4 show that the force allocation approach presented in this paper combined with the directional controller (33) is able to steer the USM towards and along the desired path.

5. CONCLUSIONS AND FUTURE RESEARCH

This paper has presented the underwater swimming manipulator, and discussed how this hyper-redundant AUV can contribute in the field of subsea IMR. The kinematics and the dynamic equations of motion for the USM were developed. This was done by extending the model of a USR by accounting for the different mass and different length of each link, and accommodating the forces and moments from additional effectors. A generic force allocation method for the highly articulated USM was proposed, and the force allocation matrix was derived, paying particular attention to the changing relative position between the CM of the USM and the center of each link. The proposed method was applied to a path following control problem, and simulation results were presented to demonstrate the extended dynamic model and the applicability of the proposed force allocation method.

In the future, the authors will investigate the applicability of the proposed path following approach for arbitrary paths, other optimization criteria, and the optimal number and placement of the additional effectors. Extended simulations with variable length and mass, and verification using experimental results, will also be further pursued.

REFERENCES

Andersson, U. (2013). *Automation and Traction Control of Articulated Vehicles*. Ph.D. thesis, Luleå University of Technology.

Antonelli, G. (2014). *Underwater Robots*. Springer International Publishing, 3 edition.

Berge, S. and Fossen, T. (1997). Robust control allocation of overactuated ships: Experiments with a model ship. In *Proc. IFAC Conf. on Manoeuvring and Control of Marine Craft (MCMC)*. Brijuni, Croatia.

Durham, W. (1993). Constrained control allocation. *Journal of Guidance, Control and Dynamics*, 16(4), 717–725.

Fossen, T.I., Johansen, T.A., and Perez, T. (2008). *Underwater Vehicles*, chapter 7: A Survey of Control Allocation Methods for Underwater Vehicles, 109–128. Inzartsev, A. V. InTech.

Fossen, T.I. and Sagatun, S.I. (1991). Adaptive control of nonlinear systems: A case study of underwater robotic systems. *Journal of Robotic Systems*, 8(3), 393–412.

Fossen, T. (1991). Adaptive macro-micro control of nonlinear underwater robotic systems. In *Proc. 5th Int. Conf. on Advanced Robotics (ICAR)*, 1569–1572. Pisa, Italy.

Fu, Y.P., Cheng, Y.H., Jiang, B., and Yang, M.K. (2011). Fault tolerant control with online control allocation for flexible satellite attitude control system. In *Proc. IEEE Int. Conf. on Intelligent Control and Information Processing*, 42–46. Harbin, China.

Gilmour, B., Niccum, G., and O'Donnell, T. (2012). Field resident AUV systems - Chevron's long-term goal for AUV development. In *Proc. IEEE/OES Autonomous Underwater Vehicles (AUV)*, 1–5. Southampton, England.

Indiveri, G. and Parlangeli, G. (2006). On thruster allocation, fault detection and accommodation issues for underwater robotic vehicles. In *Proc. Int. Symp. on Communications, Control and Signal Processing*. Marrakech, Morocco.

Jin, J., Park, B., Park, Y., and Tahk, M.J. (2006). Attitude control of a satellite with redundant thrusters. *Aerospace Science and Technology*, 10(7), 644–651.

Johansen, T. and Fossen, T. (2013). Control allocation - a survey. *Automatica*, 49(5), 1087–1103.

Johansen, T., Fuglseth, T., Tøndel, P., and Fossen, T. (2008). Optimal constrained control allocation in marine surface vessels with rudders. *Control Eng. Practice*, 16(4), 457–464.

Kelasidi, E., Pettersen, K.Y., and Gravdahl, J.T. (2014a). A waypoint guidance strategy for underwater snake robots. In
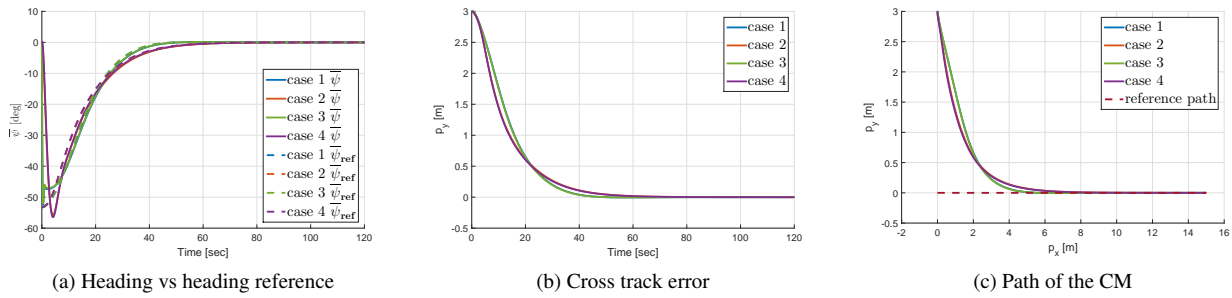
(a) Heading vs heading reference   (b) Cross track error   (c) Path of the CM

Fig. 3. Simulation results for LOS path following controller for different configurations.

(a) Case 1   (b) Case 2
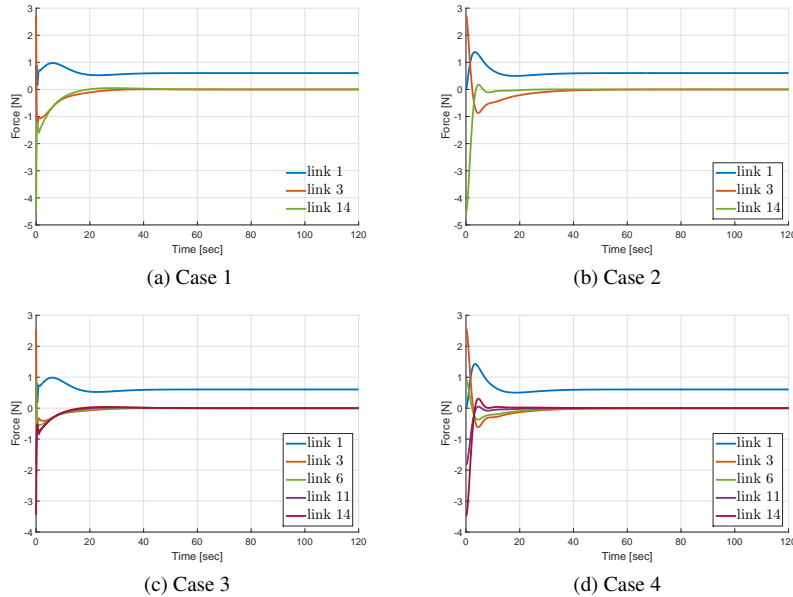

(c) Case 3   (d) Case 4

Fig. 4. Effector forces

Proc. IEEE 22nd Mediterranean Conference on Control and Automation, 1512–1519. Palermo, Italy.

Kelasidi, E., Pettersen, K.Y., Gravdahl, J.T., and Liljebäck, P. (2014b). Modeling of underwater snake robots. In *Proc. IEEE International Conference on Robotics and Automation (ICRA)*, 4540–4547. Hong Kong, China.

Kelasidi, E., Pettersen, K.Y., Liljebäck, P., and Gravdahl, J.T. (2014c). Integral line-of-sight for path-following of underwater snake robots. In *Proc. IEEE Multi-Conference on Systems and Control*, 1078 – 1085. Juan Les Antibes, France.

Khalil, W., Gallot, G., and Boyer, F. (2007). Dynamic modeling and simulation of a 3-D serial eel-like robot. *IEEE Trans. Syst., Man, Cybern. C*, 37(6), 1259–1268.

Liljebäck, P., Pettersen, K.Y., Stavdahl, Ø., and Gravdahl, J.T. (2013). *Snake Robots: Modelling, Mechatronics, and Control*. Advances in Industrial Control. Springer-Verlag.

Lindfors, I. (1993). Thrust allocation method for the dynamic positioning system. In *Proc. 10th Ship Control Symposium*, 93–106. Ottawa, Canada.

Marani, G., Choi, S.K., and Yuh, J. (2009). Underwater autonomous manipulation for intervention missions AUVs. *Ocean Engineering*, 36(1), 15 – 23.

McIsaac, K. and Ostrowski, J. (1999). A geometric approach to anguilliform locomotion: modelling of an underwater eel robot. In *Proc. IEEE International Conference on Robotics and Automation (ICRA)*, 2843–2848. Detroit, MI.

Oppenheimer, M.W., Doman, D.B., and Bolender, M.A. (2010). *The Control Handbook, Control System Applications*, chap-ter 8: Control Allocation. CRC Press, 2nd edition.

Porez, M., Boyer, F., and Ijspeert, A. (2014). Improved Lighthill fish swimming model for bio-inspired robots: Mod-eling, computational aspects and experimental comparisons. *The International Journal of Robotics Research*, 33(10), 1322–1341.

Ridao, P., Carreras, M., Ribas, D., Sanz, P., and Oliver, G. (2014). Intervention AUVs: The Next Challenge. In *Proc. 19th IFAC World Congress (IFAC-WC)*, 12146–12159. Cape Town, South Africa.

Schjølberg, I. and Fossen, T. (1994). Modelling and control of underwater vehicle-manipulator systems. In *Proc. 3rd Conf. on Marine Craft Maneuvering and Control (MCMC)*, 45–57. Southampton, UK.

Sørdalen, O.J. (1997). Optimal thrust allocation for marine vessels. *Control Eng. Practice*, 5(9), 1223–1231.

Uhlen, K., Nyman, P., Eklov, J., Laine, L., Sadeghi Kati, M., and Fredriksson, J. (2014). Coordination of actuators for an A-double heavy vehicle combination using control allo-cation. In *Proc. IEEE 17th Int. Conf. on Intelligent Trans-portation Systems (ITSC)*, 641–648. Qingdao, China.

Webster, W. and Sousa, J. (1999). Optimum allocation for multiple thrusters. In *Proc. 9th International Offshore and Polar Engineering Conference*, 83–89. Brest, France.

Yang, X. (2012). Optimal reconfiguration control of the yaw stability of the tractor-semitrailer vehicle. *Mathematical Problems in Engineering*, 2012(Article ID 602502).